PAPER

3D graphene-cellulose nanofiber hybrid scaffolds for cortical reconstruction in brain injuries

To cite this article: Do Won Hwang *et al* 2019 *2D Mater.* **6** 045043

2D Materials

RECEIVED
22 December 2018

REVISED
24 July 2019

ACCEPTED FOR PUBLICATION
5 August 2019

PUBLISHED
5 September 2019

PAPER

3D graphene-cellulose nanofiber hybrid scaffolds for cortical reconstruction in brain injuries

Do Won Hwang[1,2,3,10], Jong Bo Park[4,5,10], Dongchul Sung[6], Subeom Park[4], Kyung-Ah Min[6], Kyu Wan Kim[1], Yoori Choi[1], Han Young Kim[1], Eunji Lee[1,8], Han Soo Kim[1], Mo Ses Jin[1], Minsung Park[7], Yoo Sung Song[1], Jinwoo Park[6], Jinho Hyun[7], Suklyun Hong[6], Sung-Pyo Cho[4], Byung Hee Hong[4,5,9] and Dong Soo Lee[1,8,9]

[1] Department of Nuclear Medicine, Seoul National University Hospital, Seoul National University College of Medicine, Seoul, 03082, Republic of Korea
[2] Medical Research Center, Institute of Radiation Medicine, College of Medicine, Seoul National University, Seoul, 08826, Republic of Korea
[3] Center for Systems Biology, Massachusetts General Hospital, Harvard Medical School, Boston, MA, United States of America
[4] Department of Chemistry, College of Natural Science, Seoul National University, Seoul, 08826, Republic of Korea
[5] Biographene Inc., 1-Gwanak-ro, Gwanak-gu, Seoul 08826, Republic of Korea
[6] Graphene Research Institute, Department of Physics, and GRI-TPC International Research Center, Sejong University, Seoul, 05006, Republic of Korea
[7] Department of Biosystems and Biomaterials Science Engineering, Seoul National University, Seoul, 08826, Republic of Korea
[8] Department of Molecular Medicine and Biopharmaceutical Sciences, Graduate School of Convergence Science and Technology, and College of Medicine or College of Pharmacy, Seoul National University, Seoul, Republic of Korea
[9] Author to whom any correspondence should be addressed.
[10] These authors contributed equally to this work.

E-mail: dsl@plaza.snu.ac.kr (D S Lee) and byunghee@snu.ac.kr (B H Hong)

Keywords: graphene oxide, bacterial cellulose, cortex-mimetic 3D hybrid scaffold, corticectomized rat, photoacoustic

Supplementary material for this article is available online

Abstract

Designing the nature-driven 3D scaffold is essential for reconstructing of the injured brain in association with stem cell replacement therapy. In this paper, we developed brain cortex-mimetic 3D hybrid scaffolds and applied them to a motor-cortectomy rat model. Graphene oxide bacterial cellulose (GO-BC) hybrid scaffold integrated GOs stably and homogeneously within BC nanofibrous building blocks made of BC and amphiphilic comb-like polymers (APCLP). Density functional theory calculations and molecular dynamics simulations revealed higher binding energies between GO-BC and APCLP than between GO or APLCP with BC. The monodispersed human neural stem cells (F3 cells) incorporated within the GO-BC scaffold generated a large number of differentiated neurons with robust neurite outgrowths and possible synapse formation *in vitro*. In corticectomized rats and nude mice, highly sensitive photoacoustic signals visualized the GO-BC at the implant site. Moreover, the implanted F3 cells within GO-BC were found to survive/proliferate and differentiate to neuronal lineage from the showing neuronal and synapse markers shown on *ex vivo* immunofluorescence staining in bioluminescence imaging. Cortex-mimetic and stem cell-instructive monodisperse GO-BC hybrid scaffolds are likely to be appropriate nanoplatforms for stem cell implantation to reconstruct injured/lost brain tissues and actively differentiate neural stem cells.

Introduction

Stem cell replacement therapy has augmented the brain's inherent circuit and introduced possible new therapeutics for neurodegenerative diseases and acute brain trauma [1–3]. Amid a remarkable progress in regenerative medicine creating functional and living tissues, brain reconstruction by tissue engineering required a choice among proper cell types and a favorable environment similar to an intact brain for remodeling of the injured brain. A lack of brain-mimetic with such a sophisticated architecture nearly obliterated the reconstruction efforts to repair damaged brain tissues.

The cell-based therapy has many challenges like low survival rate of implanted cells, insufficient differentiation efficacy, and lack of long-term cell monitoring *in vivo*, which prevented any easy translational

cell-therapy for neurodegenerative diseases [4]. Once a novel variety of scaffolds were proposed, concomitant innovative imaging methods were also proposed to prove the enhanced therapeutic efficacy of these cell/scaffold complex. Additionally, a poly-l-lactic acid (PLLA) scaffold was readily available, which could prolong the viability of implanted neural stem cells in injured brain rat models [5]. However, PLLA scaffolds by themselves lacked the ability to induce stem/progenitor cells' differentiation onto neurons without attaching differentiation-inducing genes or growth factors on their surface.

Graphene, which has the versatile advantages of transparency and ultrafast conductor capacity [6–8], recently began to be used for biomedical applications as highly sensitive nanosensors, drug delivery carriers, imaging tools or substrates for regenerative medicine [9–13]. Interestingly, graphene was reported to have the potential to facilitate neuronal differentiation in neural stem cells by showing a higher amount of differentiated neurons on graphene film than on glass within 6 d [13]. Since this report, many investigators observed the graphene's capability to control stem cell fate on their own without help of any biochemical inducers [14–17]. These reports constructed a two-dimensional (2D) environment using graphene film to show graphene-induced differentiation. Using three-dimensional (3D) graphene-nanoparticle hybrid systems, Solanki *et al* observed that graphene had induced axonal alignment and neuronal differentiation [18]. Recently, Xiao *et al* and many other groups also have intensively reported the possibility of the graphene-based 2D/3D scaffolds with various types for damaged neuronal regeneration, showing the experimental results by neuronal cells and rat models [41–46]. Thus, an *in vivo* study using graphene in a disease model is warranted to test the possibility of graphene use for regenerative therapy.

In this study, we developed a transplantable 3D hybrid graphene scaffold to use *in vivo* that might be applied for future practical use in regenerative therapy. We applied this to an animal model of a traumatic brain injury where a nanocomposite, bacterial cellulose was adopted.

Bacterial cellulose (BC) was reported to have excellent properties like high elastic modulus and good biocompatibility [19, 20]. Nanofiber BC has been used as a natural extracellular matrix scaffold for cartilage engineering, blood vessel remodeling, and damaged bone repair [21, 22]. Thus, nanofiber BC can be used as a backbone to build up nanocomposite with the carbon graphene oxide sheet. Until now, it was hard to explain the binding behavior between graphene and organic molecules or polymers such as BC, amphiphilic comb-like polymers (APCLP), or membranes due to the complexity of interfaces. Theoretical studies were performed for the carbon nanotube (CNT)-polymer complex or graphene-membrane system [23, 24], but little attention was given to their interfaces. Density functional theory (DFT) calculations and molecular dynamics (MD) simulations were warranted as they help understand the binding strengths and geometrical configurations at the interfaces for graphene oxide-BC (GO-BC) nanocomposites and phospholipids or APCLP linkers.

As *in vivo* molecular imaging monitors the *in vivo* behavior of the implanted stem cells in living subjects, this could easily reveal the distribution, survival, proliferation and even functional outcomes of the implanted stem cells incorporated within graphene nanocomposites. Therefore, luciferase-based optical imaging was the ideal cell tracking method due to its low background and high sensitivity. In addition, when we use graphene, hybrid photoacoustic imaging (PAI) signals could be acquired by near-infrared (NIR) laser excitation to follow up the graphene-based nanocomposites persistence.

In this study, we produced the transplantable brain-mimetic hybrid GO-BC scaffold with adjustable elasticity and investigated whether this GO-BC scaffold might be proper as a differentiation-stimulating material in the corticectomy rat model (figure 1). Serial monitoring of implanted neural stem cells within GO-BC scaffold revealed the supportive effect of the GO-BC scaffold for the stem cell survival and proliferation/differentiation.

Results

Physical characteristics of GO-BC scaffolds

First, we prepared 300–600nm-sized GO flakes (supplementary figure 1 (stacks.iop.org/TDM/6/045043/mmedia)) by a chemical exfoliation method, and characterized their chemical and physical properties by XPS, FT-IR, and zeta potential. The GO flakes have highly negative zeta potential (avg. −34.5 mV), consisting of 39.2% of oxygen and 60.8% of carbon with O–C=O, C=O, C–O, and C=C bonds (supplementary figures 2 and 3).

The highly porous GO-BC hybrid 3D nanofiber scaffolds (GO-BC) were prepared by using a living microorganism in a simple and bio-friendly method. By adding GO flakes into the BC culture media during bacterial synthesis, the cellulose chains were expected to be more homogeneously hybridized with carbon-based nanomaterials. To guarantee uniform dispersion of GO flakes in the BC scaffold, water soluble APCLP were utilized, which have long hydrophobic (methyl methacrylate, MMA) backbones and short hydrophilic (hydroxyl-poly (oxyethylene) methacrylate (HPOEM)) and (poly (oxyethylene glycol) methacrylate (POEM)) side chains. The hydrophobic parts enabled APCLP to adhere to the GO planes while the hydrophilic parts enhanced the GO flake dispersion in aqueous medium as well as maintained GO-BC hybrid scaffold uniformtiy.

Figure 2(A) showed the morphology of the pristine BC and the GO-BC scaffolds on the left and right

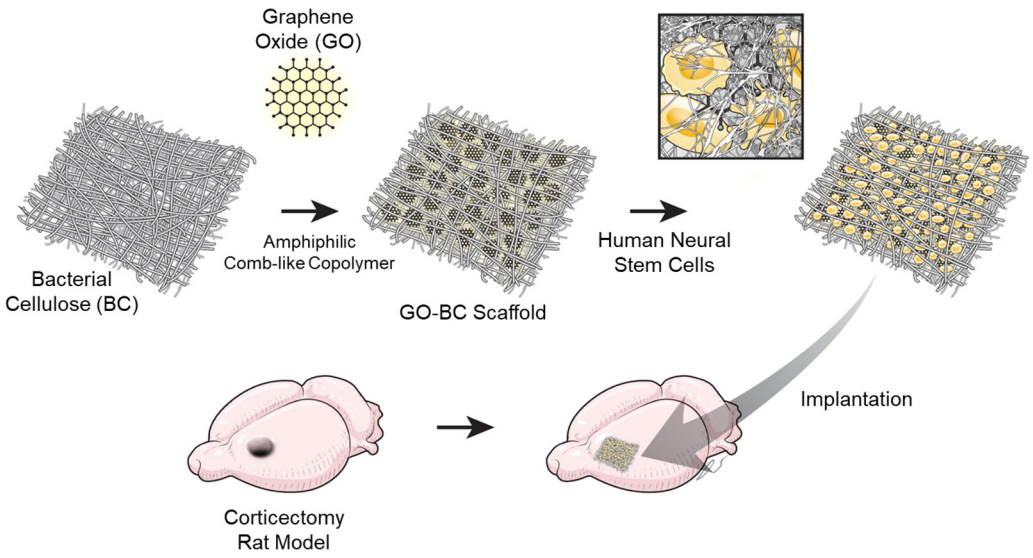

Figure 1. Schematic illustration of 3D hybrid GO-BC scaffold and application to the brain injury model. The 3D hybrid graphene oxide (GO) and BC scaffold was biosynthesized using APCLP. Human neural stem cells adhered to GO-BC hybrid scaffold were implanted into motor cortex-ablated area in a corticectomy rat model.

columns, respectively. Both BC and GO-BC scaffolds showed BC nanofibers of 30–50 nm diameters through SEM images. However, only the GO-BC scaffold showed the hybrid membrane-like plate mixture of GO flakes and BC nanofibers, which resulted in increased surface areas. The top view (upper and middle rows) showed GO-BC as more porous and loose than pristine BC. When we measured the porosity of the scaffolds by calculating the ratio of the surface area per mass using the Brunauer–Emmett–Teller (BET) theory, the higher surface area per volume and the higher porosity showed that the GO-BC scaffold had higher porosity than the pristine BC scaffold. The cross-sectional view (lower row) showed both the pristine BC and GO-BC scaffolds had layer-by-layer structure.

FT-IR spectroscopy confirmed that GO flakes of the GO-BC scaffold had peaks at 1032 and 1713 cm^{-1} representing the C=C double bond and C=O bond of the carboxylic group of GO, respectively (figure 2(B)). On the other hand, peaks at 1050, 1405, and 1627 cm^{-1} represented the C–OH, –OH and C=C bonds of BC, respectively. Using Raman spectroscopy for GO-BC, the Go distribution in BC scaffolds was measured to show the D-peak at 1350 cm^{-1} and G-peak at 1580 cm^{-1} (supplementary figure 4). The G-peak signal intensities of the GO-BC were homogenously distributed throughout the entire scaffold when mapping the G peak intensity (figure 2(C)). The mechanical strengths of BC and GO-BC scaffolds measured by AFM revealed that the GO-BC scaffold had lower Young's modulus (2.95 kPa) than pristine BC (10.39 kPa), which is compatible with the higher porosity of GO-BC (figure 2(D)).

We measured the thermal weight loss of GO, BC and GO-BC scaffolds by a thermogravimetric analysis (TGA). After heating, the weight loss of the Go flakes, BC and GO-BC scaffolds are 76.4%, 88.8%, and 88.0%, respectively. And 18.8% of the total weight of the GO flakes has remained at 800 °C. The difference of weight loss between BC and GO-BC scaffolds is about 0.8%, corresponding of remaining GO. Thus, the result indicates that the GO-BC scaffold consists of 4.3% of GO flakes and 95.7% of BC (supplementary figure 5).

Interaction affinity between phospholipid membranes and GO-BC

The membrane is composed of two-pronged lipid molecules, that have tails and heads consisting of choline-phosphate-glycerol. We considered the hybrid structures of membrane and GO with/without BC to understand their binding behaviors and performed the DFT calculations for these structures. Figure 3 showed the optimized geometries of the hybrid structures for phospholipid membranes (A) on the BC surface, (B) GO monolayer, and (C) the stacked layers of BC and GO. Table 1 listed the binding energies for these three hybrid systems. The binding energies of phospholipid membrane upon the BC, GO or GO-BC layers were defined as follows,

$E_b = -(E_{ads/sub} - E_{ads} - E_{sub})$, where $E_{ads/sub}$, E_{ads}, E_{sub} represented total energies of phospholipid/substrate, phospholipid, and substrate, respectively. The substrate represented BC, GO, and GO-BC, which correspond to figures 3(A)–(C), respectively. The binding energies of phospholipid layers were 0.87, 0.42, and 1.07 eV per unit cell on BC, GO, and GO-BC, respectively. This implied that phospholipid layers were more strongly adsorbed on the BC with GO than on BC or GO alone.

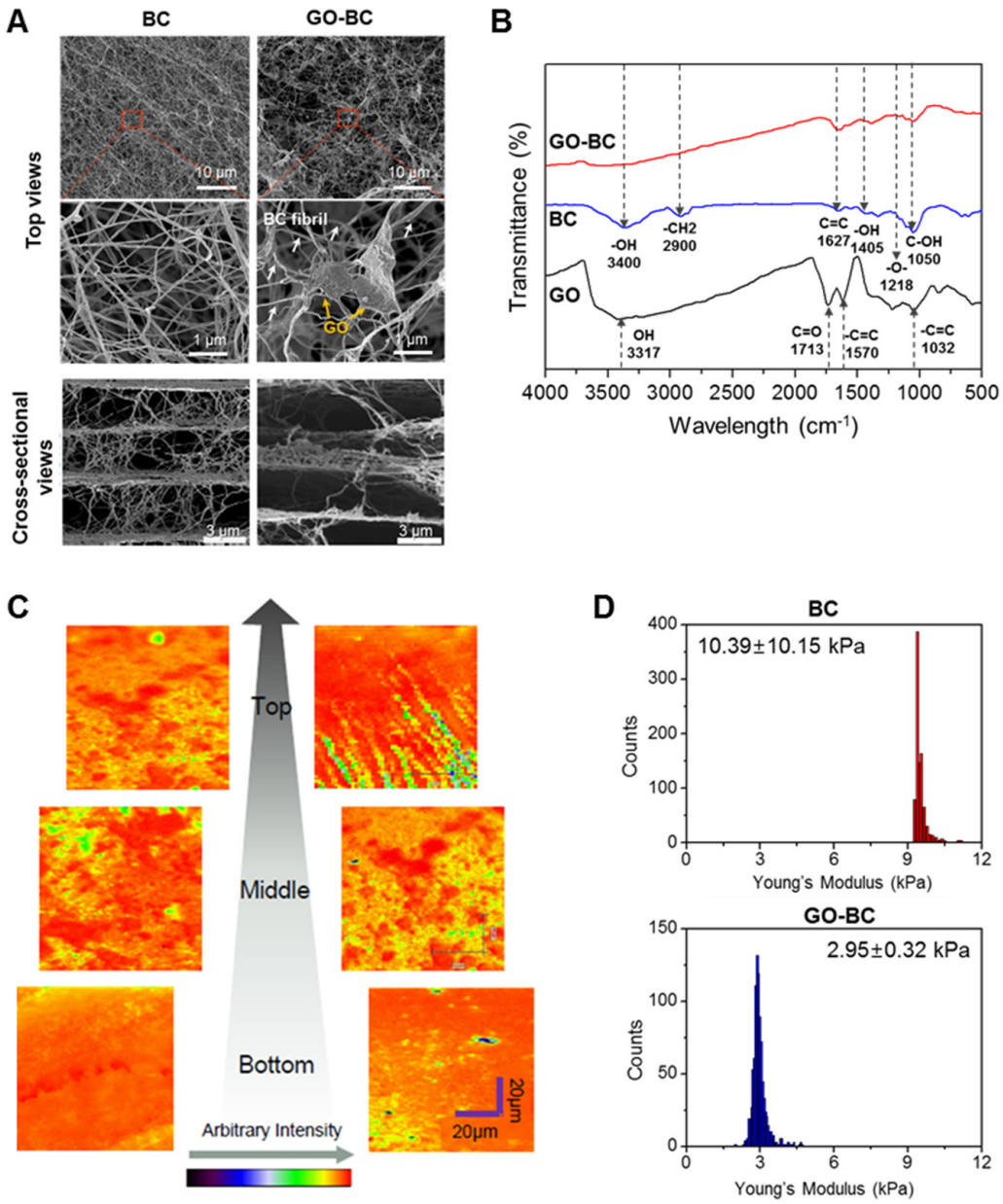

Figure 2. Morphological, chemical, and mechanical characterization of GO-BC hybrid scaffold. (A) Low- and high-magnified FE-SEM images of pristine BC and bio-synthesized GO-BC scaffolds. Scale bars, 10, 1 μm (top view), and 3 μm (cross-sectional view). The white and yellow arrows indicate the BC fibrils and GO flakes, respectively. (B) FT-IR spectrum of GO flakes (black), BC (blue), and GO-BC (red) scaffolds. (C) G-peak intensity Raman mapping in the GO-BC showed the homogenous distribution of G-peak signal intensities with uniformly dispersed GO flakes in the GO-BC scaffold. The top, middle, and bottom images were measured from the same scaffold, with different area. (D) The mechanical properties of BC and GO-BC scaffolds were measured by AFM, showing lower Young's modulus in GO-BC than the pristine BC.

Interaction affinity of GO-BC-APCLP hybrids on MD simulation

We performed DFT calculations for the GO hybrids with BC and APCLP. Table 2 showed the binding energies E_b and the nearest interatomic distance d_{ni} between adsorbate and substrate in the GO hybrids. The binding energies of adsorbates are defined by the following equation for these GO hybrids: $E_b = -(E_{ads/sub} - E_{ads} - E_{sub})$, where $E_{ads/sub}$, E_{ads}, and E_{sub} represented total energies of the GO hybrid adsorbate/substrate system, adsorbate, and substrate, respectively. Each adsorbate and substrate corresponding to figure 3 was provided in table 2. DFT calculations showed that binding energies of BC and APCLP with GO were 0.69 and 0.77 eV per unit cell, respectively, with 2.09 and 2.10 Å as the nearest atomic distance between them. In case of BC adsorbate with APCLP-coated GO, the binding energy of BC was 0.85 eV per unit cell with the nearest atomic distance of 2.05 Å. Our calculations implied that the interaction between BC and GO was enhanced by APCLP since BC interacted more strongly with APCLP-coated GO with increased binding energy of 0.16 eV per unit cell.

The MD simulation for GO-BC hybrid showed that pieces of BC were close to each other, but not as close as the BC in the absence of GO (figure 3(D)), because pieces of BC interacted more strongly with GO than with themselves. MD simulation showed that pieces of

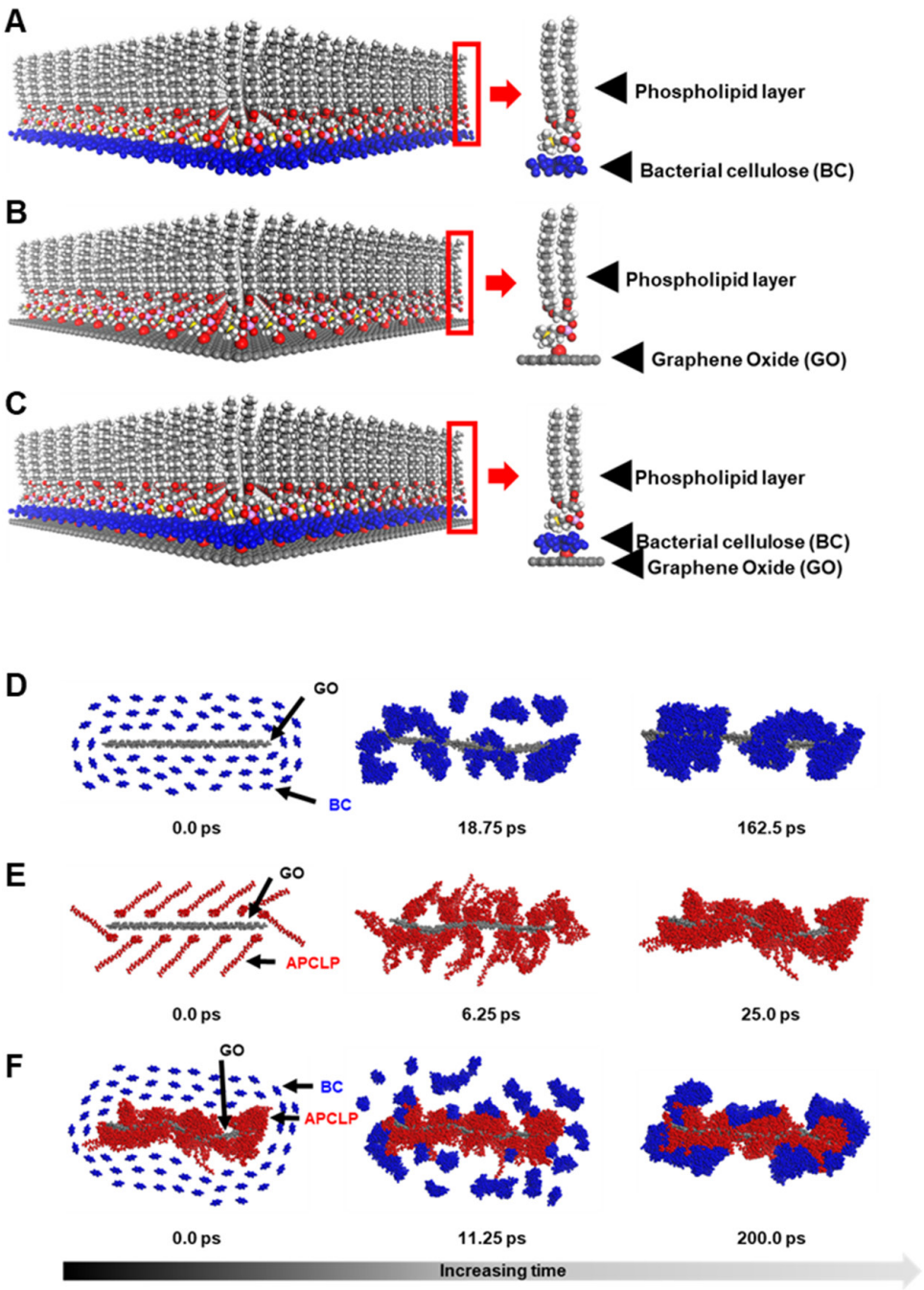

Figure 3. Interaction affinity of GO-BC hybrid scaffold with phospholipid layer and APCLP on DFT and MD calculations. (A)–(C) Optimized geometries of phospholipid layer on BC, graphene oxide (GO), and the stacked structure of BC and GO by DFT calculations. Each unit-cell is represented by a red rectangle on the right side of the geometry. The dark gray, red, pink, and yellow balls represent the carbon, oxygen, phosphorus, and nitrogen atoms, respectively. The blue cloud-like structures indicate the BC. (D)–(F) MD simulations for GO-BC, GO-APCLP, and APCLP-coated GO-BC according to variations in time. Gray, blue, and red structures indicate GO, BC, and APCLP, respectively.

Table 1. Binding energies (in units of eV) of phospholipid layers are obtained by DFT calculations.

Substrate	BC	GO	BC/GO
E_b (eV/unitcell)	0.87	0.42	1.07

Table 2. Binding energies of adsorbate on substrate and nearest interatomic distance (d_{ni}) are obtained by DFT calculations.

Adsorbate	BC	APCLP	BC
Substrate	GO	GO	APCLP + GO
E_b (eV/unitcell)	0.69	0.77	0.85
d_{ni} (Å)	2.09	2.10	2.05

BC tended to move toward the GO functional groups such as –COOH or –OH, thus, GO functional groups were supposed to play essential roles in the interaction between GO and BC. MD simulation for GO-APCLP (figure 3(E)) showed that GO was covered by APCLP layers as the hydrophilic head group of APCLP moved towards GO functional groups. Then, MD simulations for BC and APCLP-coated GO by using the APCLP-GO

hybrid geometry (figure 3(F)) showed that BCs moved towards APCLP-coated GO and became seated. The APCLP-coated GO interaction with BC was due to the presence of APCLP, which enhanced the GO binding with BC. These behaviors in MD simulations were well matched with the experimental observations where APCLP acted as an adhesive between GO and BC. Further simulation revealed that BC interacted with APCLP-coated GO due to the presence of APCLP.

In figures 3(D)–(F), we obtained the structures of GO-BC, GO-APCLP, and APCLP-coated GO-BC according to the variation in time; initial (left), transition (middle), and equilibrium (right) states. Here, the time scales for reactions can be different in the MD simulations, because each system in figures 3(D)–(F) consists of different kind and number of molecules. Furthermore, we have already obtained equilibrium states for GO-BC, GO-APCLP, and APCLP-coated GO-BC in figures 3(D)–(F) (see the rightmost figures of figures 3(D)–(F), which represent the equilibrium states). So, even though we consider a longer time scale in the MD simulations, we can expect that there are no significant changes from the equilibrium states shown in the rightmost figures of figures 3(D)–(F).

Proliferation and morphological changes of human neural stem cells within GO-BC scaffolds *in vitro*

The human neural stem cell line, F3-effluc cells stably express the enhanced firefly luciferase (effluc) gene via codon optimization and Thy1.1 (CD90.1) in retroviral backbone. FACS analysis for CD90.1$^+$ F3-effluc cells collected via MACS showed that the effluc gene-infected cells were over 90% (data not shown). BC and GO-BC were punched to yield globular scaffold (diameter: 8 mm, thickness: 0.5 mm) while human neural stem cells (F3-effluc cells) were incorporated into this sterile globular GO-BC scaffolds. The cells were slowly treated to GO-BC scaffold where the morphology was found to be changed even 2 d after incorporation on the GO-BC scaffold (lower row of figure 4(A)). The phase contrast images showed thin and long neurites grown from these neural stem cells within the GO-BC scaffold (figure 4(A) left column). In contrast, the cells incorporated within the BC scaffold maintained their round shape in 3D architecture. This difference was obvious in DiI-labeled F3-effluc cells (figure 4(A) right column).

F3-effluc cells with complete medium were slowly dropped onto and under the GO-BC scaffold slap (1 cm × 1 cm × 0.5 mm) and cell/scaffold complex was incubated for a further 24 h before the distribution was examined by a 3D confocal microscopy. F3-effluc cells were homogenously distributed inside the GO-BC scaffold in a monodisperse fashion (figure 4(B)). The confocal fluorescence scanning along the *z* axis showed that cells resided mainly in the center of the GO-BC scaffold. In contrast, neural stem cells within BC scaffold were clustered while forming neurosphere-like structures on day 2 (supplementary figure 6).

F3-effluc cells within BC or GO-BC scaffolds gradually increased in number according to luciferase activity until day 8, which indicated that each scaffold provided sufficient space for cell growth (figure 4(C)). The difference between BC and GO-BC on cells is due to immunofluorescent staining of mature neuronal markers, MAP2 and synaptophysin, whose immunofluorescence was only found in F3 cells within GO-BC scaffold but not in F3 cells within BC scaffold on day 12 (figure 4(D)). Calcium imaging was conducted to measure neuronal functionality of F3 cells within GO-BC scaffold. Fluo-3 AM ester kit was used to measure calcium level based on fluorescence image *in vitro*. We found that green fluorescence signals were found in F3 cells within GO-BC, but not in F3 cells within BC scaffold (supplementary figure 7).

Cell growth within GO-BC implanted in nude mouse by *in vivo* optical and PAI

We compared *in vivo* growth pattern of F3-effluc cells within BC and GO-BC scaffolds in nude mice, against the same number implanted via subcutaneous administration. *In vivo* bioluminescence images showed a continuous increase in cell-only groups as well as in cells within both BC and GO-BC scaffolds until day 12 (figure 4(E)). The quantitative region of interest (ROI) analysis showed that proliferation rates were grossly similar with the highest in cells within GO-BC scaffold and lowest in cells within BC scaffold.

GO absorbs NIR strongly and enables us to acquire photoacoustic signals. The photoacoustic/ultrasound images were acquired in nude mice with subcutaneously inoculated GO-BC/cell complex. After the correct localization of implant sites with high resolution using ultrasound mode, intense photoacoustic signals were observed only in the GO-BC/cell complex-implanted region on PAI mode (figure 4(F)). The U-shaped folding of GO-BC scaffold seen on PAI was similarly found on days 4 and 8 through luciferase imaging in figure 4(E). Non-specific false positive photoacoustic signals in the sites inoculated with BC/cell complex and cell only were found in the surrounding area of the injected site (subcutaneous area) of mouse possibly owing to the unexpected bleeding.

Signals measured on each day of PAI imaging were the same until day 12, which indicated that implanted GO-BC scaffold stayed in the implanted site until that day (supplementary figure 8). The hematoxylin and eosin (H&E) staining of the complexes showed central necrosis in cell-only groups. In contrast, cells within BC or GO-BC scaffolds were highly proliferative and homogeneous in distribution, which implied that BC or GO-BC scaffolds enabled a sufficient supply of oxygen and substrates (supplementary figure 9).

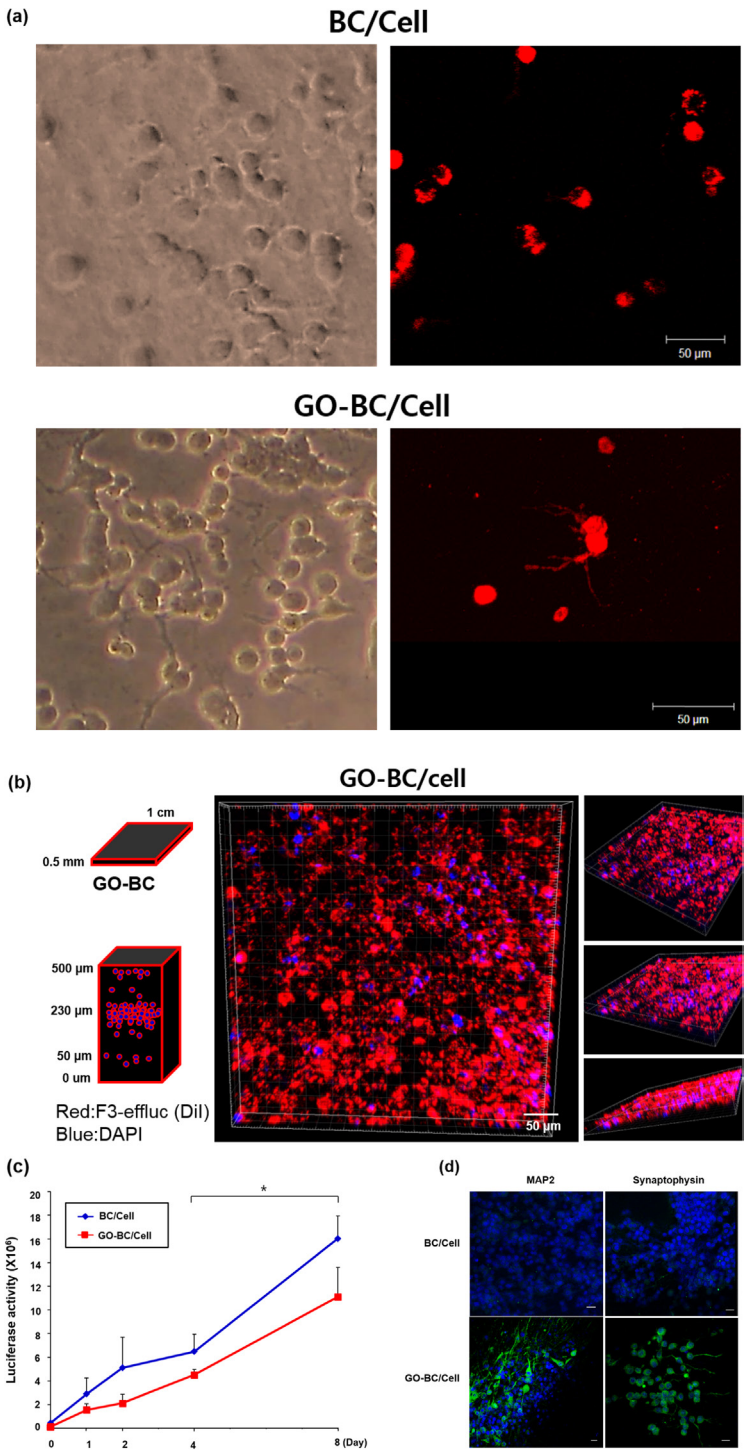

Figure 4. Rapid attachment and growth of F3-effluc neural stem cells within GO-BC scaffold. (A) Phase contrast and confocal microscopy images of DiI-labeled F3-effluc cells 2 d after incubation in each scaffold. The neurite outgrowth of F3-effluc cells in GO-BC scaffold are shown in the GO-BC scaffold group, compared to cells in BC scaffold. (B) 3D confocal microscope images of DiI-labeled F3-effluc cells on scaffold (Red: DiI for cell labeling, Blue: DAPI for nucleus staining). F3-effluc cells were mainly distributed in the inner layer of GO-BC scaffold. (C) Serial luciferase activity was examined in F3-effluc cells within either BC or GO-BC scaffold. The F3-effluc cells on GO-BC scaffold were gradually grown for 8 d ($n = 5$). (D) Immunofluorescence staining of human neural stem cells incorporated within GO-BC hybrid scaffold. Cells were fixed using 4% PFA, where mature neuronal marker, MAP2 and synaptophysin protein were highly expressed only in the cytoplasmic area of F3-effluc cells within GO-BC scaffold after 12 d. Scale Bar, 10 μm. (E) *In vivo* time course bioluminescence images were acquired in GO-BC/cell, BC/cell, and cell only (F3-effluc)-implanted mouse groups ($n = 5$) for 12 d. F3-effluc cells on cells, BC/cells, and GO-BC/cell groups showed gradual increases in their cell growth for 12 d. The quantitative region of interest (ROI) assay was measured and signal intensity was represented as radiance (p/sec/cm^2/sr), which refers to the number of photons per second over a square centimeter of tissue radiating into a solid angle of one steradian (sr). Exposure time was 30 s. (F) Photoacoustic (PA)/ultrasound (US) images were obtained in nude mice subcutaneously implanted with GO-BC/cell, BC/cell, and cells ($n = 3$) for 12 d. Red color shows PA signals emitted from GO-BC scaffold. 700 nm PA laser excitation, 40 db of photoacoustic gain. GO-BC scaffold showed intense photoacoustic signals for 12 d when compared to F3-effluc cell-or BC/cell-injected region. Quantification data from PA intensity of each region showed PA intensity of GO-BC scaffold was maintained for 12 d and was about 5 times greater than other groups.

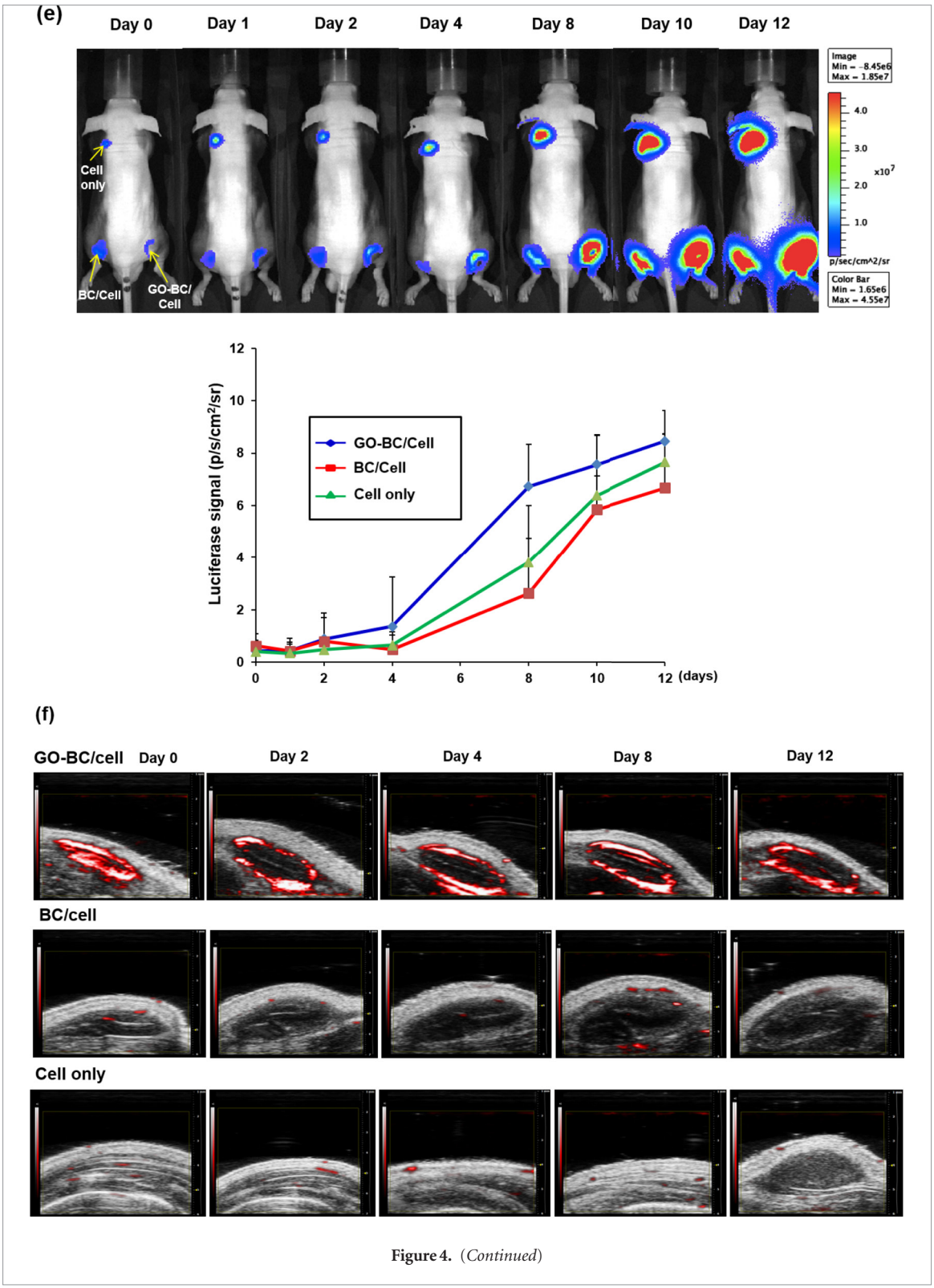

Figure 4. (*Continued*)

Prolonged viability of neural stem cells within BC or GO-BC scaffolds implanted in motor-corticectomy rat model

F3-effluc cells within 3D hybrid GO-BC scaffold were implanted to motor cortex-ablated rats, which mimicked trauma injuries. The right motor cortex with proper coordinates were surgically removed and abnormal motor behavior was confirmed using behavior tests of proprioception fore-limb and hind-limb, whisker tactile, and visual forward. Corticectomized rats showed motor weakness 1 week after operation (supplementary figure 10). F3-effluc cells loaded onto GO-BC scaffolds and then transplanted into the ablated area of the brain showed bioluminescence, as shown in figure 5(A). This bioluminescence was supposed to represent the number of viable (and proliferating) implanted F3-effluc cells and was slightly reduced until day 2. Afterwards the time increased rapidly, representing vigorous cell growth within BC or GO-BC scaffolds

(figure 5(A) second and third rows). The proliferation was at the peak on day 8 for both BC and GO-BC scaffolds (supplementary figure 11) and sustained a little more in GO-BC scaffold. Bioluminescence signals disappeared on day 12 while in cell-only groups, bioluminescence started declining on day 4 and disappeared on day 10. Photoacoustic signals persisted in the implanted site in GO-BC/cell groups (figure 5(B) left and middle columns). Obviously, no photoacoustic signals were observed in BC/cell and cell-only implant groups (figure 5(B) right column).

Differentiation of the implanted neural stem cells toward neuronal lineage within GO-BC, but not BC scaffolds

To verify whether the F3-effluc neural stem cells incorporated within GO-BC scaffold give rise the majority of neuronal types in the injured cortex area, the brains were excised on day 8 when bioluminescence signals were observed in all three groups. GO-BC scaffolds were easily identified by the black color. Most F3-effluc cells within GO-BC scaffold showed strong homogeneous staining on MAP2 (mature neuronal marker) and synaptophysin (synaptic vesicle protein) immunohistochemistry, which indicated the cells' differentiation into neuronal lineage and formation of synapses (figure 5(C), supplementary figure 12). Few cells within BC scaffold were also stained with MAP2 or synpatophysin. In cell only-implanted groups, no MAP2 or synaptophysin-positive cells were found.

Discussion

Designing biomimetic artificial brain tissues using appropriate 3D nanocomposite scaffolds is essential for anticipating the therapeutic efficacy in repairing injured brain tissue. Multilayered nanocomposites composed of nanofibrillar BC complexes with graphene oxide can provide an appropriate 3D brain construct to replace injured/lost brain tissue. As the GO-BC scaffold used in this study had multilayered structures when co-incubated with cells *in vitro* similar to the brain, the GO-BC cell complex was used to replace and reconstruct the lost brain tissue in a corticectomy rat model. Fortunately, this GO-BC scaffold has similar mechanical elasticity as an intact brain around 1000 Pascal [25]. When it was used to help in wound healing, there was good biocompatibility and high tensile strength with no further extracellular matrix components needed for this scaffold [26].

On the other hand, it is important to confirm the interactions between the interfaces of the materials in the process of forming the nanocomposite scaffolds. For the GO and membrane hybrid systems, the binding strength of phospholipid membrane layers with GO is much enhanced when BC is intercalated between phospholipids and GO (figure 3(C)). This means that the phospholipid membrane interacts more strongly with the BC/GO combined system rather than with BC or GO itself. Moreover, GO-BC scaffolds can be well combined by APCLP which acts as an adhesive with increased binding strength between GO and BC (table 2). Such APCLP aids in the homogeneous distribution of BC nanofibers on GO by mediating the hybridization between them (figure 3(F)). In this study, GO-BC neural stem cell complex showed promising characteristics to proliferate and differentiate *in situ* at the implantation sites which might be later to reconstitute functional brain tissues. After understanding the behavior of GO-BC cell complex *in vitro*, we explored its applicability *in vivo* on corticectomized brain rat model.

Compared to the mechanically flexible 2D GO-BC film made of BC and graphene [27], 3D GO-BC scaffold used in this study had a stacked layer structure. The cell/scaffold complex was once utilized to fill in lost brain tissue [28]. The host and grafted cells within the scaffold communicate while minimizing astroglial scarring in inflammation in addition to facilitating the long-distance axonal projection from implanted cells toward host parenchyma. We observed in the rat model that GO-BC cell complex helped produce a high amount of MAP2 and synaptophysin-positive neuronal cells differentiated from F3 human neural stem cells 8 d after implantation. This is a distinct advantage of the GO-BC complex for implanted neural stem cells' nests as these differentiation markers were never found in cell-only groups or weak in few cells in the BC scaffold group. We propose that GO within GO-BC scaffold were able to stimulate the differentiation of implanted neural stem cells toward functioning neurons.

In vivo molecular imaging valuates stem cell behavior in terms of survival, migration, and proliferation [29–32]. This lets us find where the cells were localized, how long they survived, and how much they proliferated at serial imaging at as many time points as we want. For example, if we measure the bioluminescence at the implanted site in the cells expressing luciferase, we are practically quantifying the number of cells and actually watching the proliferation. Proliferating cells can leave the injection/implantation sites and this moving out or homing to other organs can also be monitored. In this study, the implanted F3-effluc neural stem cells within GO-BC scaffold were clearly visualized via bioluminescence imaging. As expected, GO of GO-BC scaffold stayed at the injection site without being released to the adjacent areas. Concomitant bioluminescence imaging and ultrasound with PAI made this observation possible.

Compared to the BC scaffold, a larger surface with wrinkles and ripples of GO in GO-BC scaffold would have caused a positive effect on the cell viability and growth as cells were adhered on the added surface of GO. The GO surface was known to interact with serum proteins and would have enhanced the cell attachment and growth [47, 48]. We speculate that micro-sized GO in GO-BC scaffold would have supplied a surface for

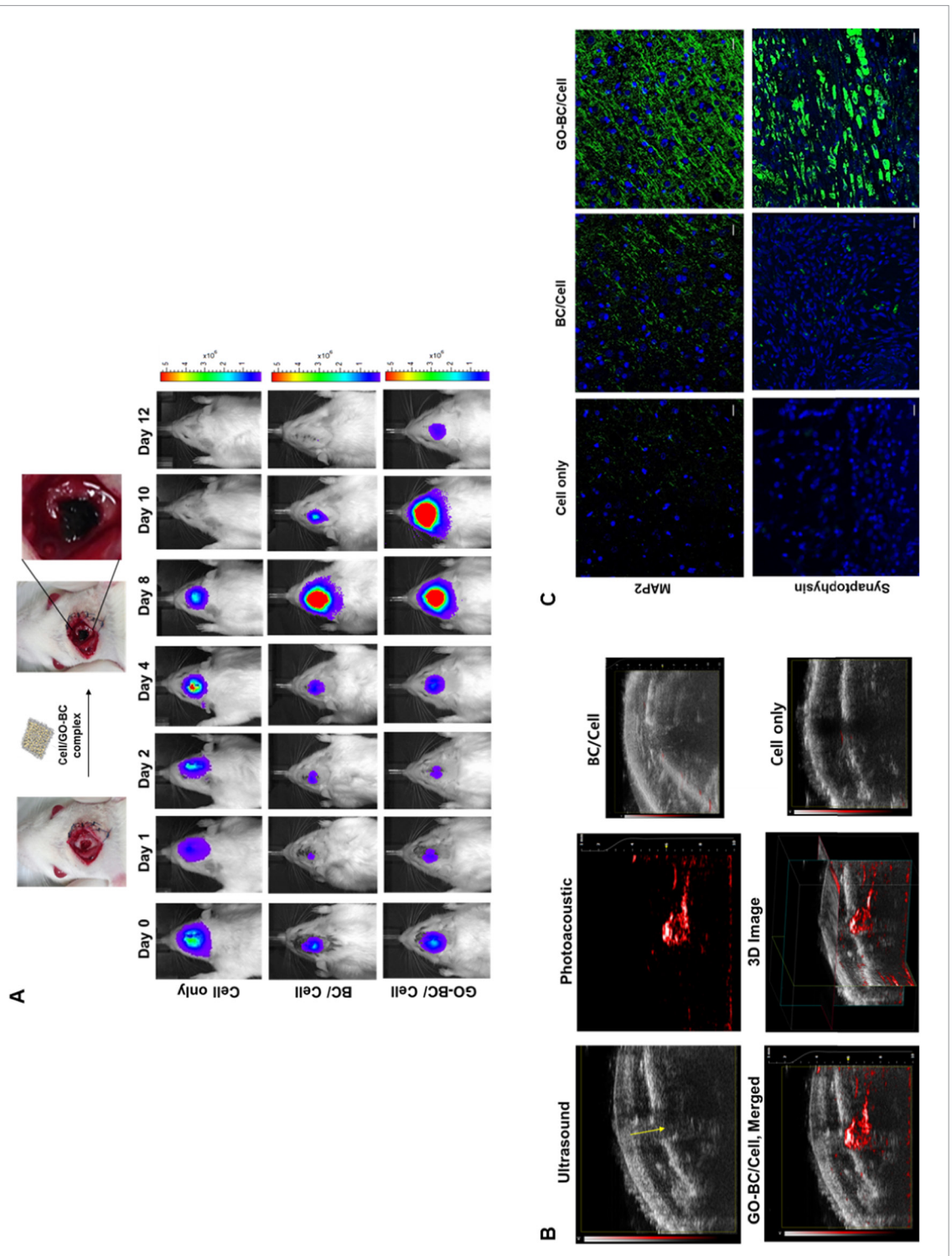

Figure 5. Visualization of the viable grafted cells and GO-BC scaffold by bioluminescence and photoacoustic image in corticectomy rat model. (A) After the 5×10^5 F3-effluc cells were incorporated into the GO-BC scaffold, the cell/scaffold complex was incubated for 2 h at 37 °C. Seven days after establishing the corticectomy rat model, cell/scaffold complex was implanted into the cavity of the injured rat brain. *In vivo* bioluminescence images were acquired after 12 d. (B) *In vivo* photoacoustic images were obtained in the corticectomy rat model transplanted with GO-BC/cell, BC/cell, or cell only. Ultrasound images showed the removed cortical cavity of a corticectomized rat. The PA signal (red) and cortex cavity area (yellow arrow) were perfectly matched in the GO-BC/cell-transplanted model. In contrast, no PA signals were observed in the cell only injected rat model. ROI results in GO-BC/cell-implanted brain region were about 2.5 times greater in PA signals than cell-treated groups. (C) Immunostaining of corticectomized rat brain on day 8 were conducted using neural markers (MAP2) and synaptic marker (synaptophysin). In GO-BC/cell group, most F3-effluc cells were MAP2 positive inside the GO-BC scaffold and showed higher MAP2 expression when compared to BC/cell group. The synaptophysin level was also high in a large number of F3-effluc cells within the GO-BC scaffold. Neither MAP2 nor synaptophysin was expressed in cell only-implanted groups.

the initial adhesion of cells. Furthermore, nanofibrous BC would have facilitated axonal elongation supplying an optimal environment for neural stem cells for reconstructing lost brain tissue. In nude mice, *in vivo* bioluminescence imaging revealed the survival and proliferation of implanted cells in the scaffolds (figure 4(E)), which was also the case in corticectomized rats (figure 5(A)). Nude mice and corticectomized rats were different in that bioluminescence was sustained in nude mice, but it peaked and faded away in rats. Unlike nude mice, immunocompetent rats would have rejected the xenografted human-origin neural stem cells despite daily administration of immunosuppressor drugs.

Strong NIR absorption and the consequent emission of heat or ultrasonic sound made the use of GO for photothermal therapy [33] or PAI possible. As GO absorbs NIR, the location of the GO-BC could be determined using PAI instruments. As expected, we observed highly sensitive photoacoustic signals of GO-BC scaffolds at the inoculation site, reflecting their shape and location in nude mice (figure 4(F)) and corticectomized rats (figure 5(B)). Merged with ultrasound images that provide explicit anatomical information, the implanted GO-BC cell complex was localized serially at several time points in nude mice. In the corticectomy rat model, we also localized the implanted GO-BC cell complex by PAI, although there were false positive signals due to hematoma/bleeding in ablated cortical cavity around the implanted area.

The critical problems for successful cell-based regenerative therapy include poor cell survival and inefficient integration into the host brain tissue, in addition to low efficacy of grafted stem cell differentiation towards functioning neurons. For reconstructing an injured brain, biomaterials are expected to (1) reduce inflammation and apoptosis for neuroprotection, (2) help reparative processes, and (3) promote neurite outgrowth as well as axonal elongation [34]. We presented a GO-BC scaffold combined with proper neural stem cells that satisfy the expected roles by both enhancing survival and facilitating differentiation *in vivo*. Integrating these GO-BC cell complex with the host brain tissue is the next step, but we do not have the capability to modify the surface of GO with nerve growth factors to promote the cooperation of the implanted cells with the neurons and glial cells of the host brain tissue.

Considering the demands to the functional scaffolds support the damaged/injured/lost brain tissue reconstruction, structurally cortex-mimicking and stem-cell supportive bioactive GO-BC hybrid scaffolds derived from bacterially-produced materials were proposed as a plausible therapeutic options. We think that the GO-BC cell scaffold, especially taking advantage of GO for its graft and differentiation-promoting capability, can yield an optimal brain microenvironment with good biocompatibility. With proper guidance, this GO-BC scaffold might be able to educate the grafted cells towards desirable cell types like specific neurons or glial cells. A proper combination of implanted cells and brain-mimetic biomaterials will enable the coordination of repair and reconstruction processes of the injured brain. However, incorporating with the host brain or overcoming the immune rejection needs further research. The immune response to BC or GO should also be investigated. The GO-BC stem cell complex might regenerate the neurons/astrocytes easier in terminally dysfunctional brains in many neurodegenerative diseases, spinal cord injuries or even regenerative muscles in cardiomyopathy to help remodel in regenerative medicine.

Materials and methods

Preparation of graphene oxide (GO) flakes

Graphene oxide flakes were prepared by Hummer's method with minor modifications. Shortly, 5 g graphite (99.9995% purification, purchased from Alfa Aesar) was poured into 169 ml sulfuric acid (95%, purchased from Sigma Aldrich), followed by adding $NaNO_3$. Then, the oxidative reagent, $KMnO_4$ was slowly poured into the mixed solution under ice bath to keep the solution temperature below 10 °C. After stirring for 5 d in ambient conditions, 15 ml H_2O_2 was poured into the mixed solution, and mild stirring was maintained for 1 more day. For purification, DI-water was added into the reaction solution, and centrifuged at 5000 rpm for 30 min. The supernatant liquid of the GO solution was removed and the rinsing process was repeated more than 15 times to eliminate the residual salts and acids completely. The GO flakes were freeze-dried and stored in a desiccator.

Preparation of GO flakes coated with APCL

The amphiphilic comb-like copolymers (APCLP) were synthesized by free radical polymerization of MMA, hydroxyl-poly(ethylene glycol) methacrylate (HPOEM), and poly(ethylene glycol) methylether methacrylate (POEM) in tetrahydrofuran for 18 h (MMA: HPOEM: POEM = 61: 21: 18). The molecular weight of the APCLP was measured approximately 25 000 Da by a gel permeation chromatography (GPC), and the polydispersity was approximately 2.7. Next, the APCLP 1mg of GO flakes was added to 10 ml of APCLP solution (0.001% in 30% ethanol), and sonicated using a horn-type ultrasonic generator (Fisher Scientific Co., USA) with a frequency of 23 kHz for 20 min in an ice bath.

Culture of G. xylinus

A mannitol media, which consists of 2.5wt% mannitol, 0.5wt% yeast extract, and 0.3wt% bacto-peptone, was sterilized at 120 °C for 20 min. *G. xylinus* (KCCM 40216) was purchased from the Korean Culture Center of Microorganisms, and pre-cultured on agar culture medium to form bacterium colonies. A *G. xylinus* single colony was transferred into a 100 ml Erlenmeyer flask filled with mannitol medium.

Preparation of BC and GO-BC scaffolds

The pre-cultured bacterium suspension was added into a mixed mannitol medium (pH 6.0) with 1×10^{-3} (w/v) dispersed GO flakes coated with APCLP, and incubated at 28 °C for 2 weeks. And the GO-BC membrane was simply biosynthesized and purified by boiling in 1 wt% NaOH solution at 90 °C for 2 h and washing with running DI-water. And it was soaked in 1 wt% NaOH solution for 1 d in ambient condition for eliminating the cell debris and residual salts and liquids. The pH of medium was then adjusted to 7.0 by washing with DI-water. Furthermore, the GO-BC scaffold was bleached by soaking in 1 wt% NaClO solution for 2 h, and washing with DI-water. Finally, the scaffold was dried at 60 °C overnight. The normal BC scaffold was prepared by harvesting a single *G. xylinus* in mannitol medium without GO flakes, purifying and bleaching as described previously.

Characterization of BC and GO-BC scaffolds

The BC and GO-BC scaffolds were freeze-dried by a freeze dryer (Bondiro, Ilshinbiobase, Korea) with below 10mTorr for 3 d for imaging. After that, they analysed by both an image analysis system (Axio Observer Z1, Zeiss, Göttingen, Germany) coupled to a light microscope and a scanning electron microscopy (SEM, JSM-6330F, JEOL) at 5 kV. In addition, transmission electron microscopy (TEM, JEOL 2100, JEOL, Japan) was operated at 200 kV to analyse GO integration. The Raman spectra were obtained from top, middle, and bottom layers of GO-BC by using a Renishaw inVia micro-Raman spectrometer (λ laser = 514 nm, ~500 nm spot size, 100 × objective).

The porosity of the scaffolds was measured by using a mercury intrusion porosimetry (AutoporeIV9500, Micromeritics Inc., Norcross, GA). Nitrogen physisorption measurements at 77 K were performed by a Quantachrome NOVA 4000 (U.S.A.). Brunauer-Emmett-Teller (BET) and Barrett-Joyner-Halenda (BJH) analyses were carried out by Autosorb software (Quantachrome). The BET analysis was conducted at a relative vapour pressure of 0.05–0.3 while the BJH analysis was carried out from the desorption branch of the isotherm.

AFM images were obtained by a Park systems XE-100 scanning probe microscope at ambient conditions, where the silicon cantilever (NSC-36, Mikromasch Inc.) with pyramidal-shaped tips (curvature radius = 10 nm) has a 0.60 N m^{-1} of spring constant. Topological images were employed using a compressive load of 10 nN during scanning. The forward and backward rates were 0.3 μm s^{-1} and 40 nN of a maximum compressive load was applied to the surface. The Young's modulus of the scaffolds was calculated by the Hertzian model while the Poisson's ratio (ν) was set to 0.5 and parabolic geometry of the indenter was set.

DFT calculation and MD simulation of GO-BC scaffold

We performed DFT calculations for several GO hybrids with BC, APCLP, and phospholipids. Our DFT calculations use generalized gradient approximation (GGA) in the Vienna *ab initio* simulation package (VASP) [35–37] where the kinetic energy cut-off is set to 400 eV. For the van der Waals (vdW) correction, we employ Grimme's DFT-D2 method, based on a semi-empirical GGA-type theory [38]. All atomic coordinates are fully relaxed until the Hellmann-Feynman forces are less than 0.025 eV $Å^{-1}$. For the Brillouin-zone integration, we use $1 \times 1 \times 1$, $3 \times 3 \times 1$ and $3 \times 1 \times 1$ for GO hybrids with BC/phospholipids, BC, and APCLP, respectively. In order to explain the binding behaviors of GO hybrids for large-scale dynamic systems, we also performed MD simulation for GO hybrids at room temperature (300 K). To perform NVT-MD simulations, we use the large-scale atomic/molecular massively parallel simulator (LAMMPS) with reactive force field (ReaxFF) potentials [39].

Cell culture and preparation of cells on GO-BC scaffold

HB1.F3 human neural stem cells were isolated from 15 week old embryonic brains and immortalized by retrovirus-mediated v-myc oncogene transduction (Kindly provided by Seung U Kim, Chung-Ang University College of Medicine). The F3 cells were cultured in Dulbecco's modified Eagle's medium (Invitrogen, Grand Island, NY), containing 10% fetal bovine serum (FBS, Invitrogen) with 10 U ml^{-1} penicillin and 10 μg ml^{-1} streptomycin (Invitrogen) in a 5% CO_2 humidified incubator at 37 °C. GO-BC preserved in isopropyl alcohol was stamped with 1 cm-diameter puncher for size modification, while was followed by extensive PBS washing to remove isopropyl alcohol. After GO-BC was loaded onto a 24-well plate, 10 μl of 5×10^4 F3-effLuc cells resuspended in PBS were incorporated into the GO-BC. 1 ml of complete medium was added to a 24 well plate after GO-BC/cell complex was incubated for 2 h.

Establishment of F3 cells stably expressing enhanced luciferase reporters

F3 cells were genetically engineered using a retrovirus system to express the codon-optimized enhanced firefly luciferase gene (effluc). Thy1.1 (CD90.1) tag is contained in the retroviral backbone based on an internal ribosome entry site (IRES) driven by a cytomegalovirus (CMV) promoter. The effluc retroviral vector and three major genes (GAG, Pol, and Env) were transfected using lipofectamine reagent (ThermoFisher. Scientific) into 293FT packaging cell lines in a 10 cm flask dish for retrovirus production. The produced retrovirus-containing supernatant was collected 2 d after transfection. The retrovirus was

added to F3 cells with 10 mM polybrene to increase viral infection efficacy and the infected F3-effluc cells were separated into $CD90.1^+$ and $CD90.1^-$ cells using monoclonal anti-CD90.1-conjugated magnetic microbeads by magnetic-activated cell sorting (MACS; Miltenyi Biotech Ltd, Bisley, Surrey, UK). The purification of $CD90.1^+$ cells were identified by FACS (BD Immunocytometry System; Becton Dickinson, CA, USA) analysis using isothiocyanate (FITC)-conjugated anti-CD90.1.

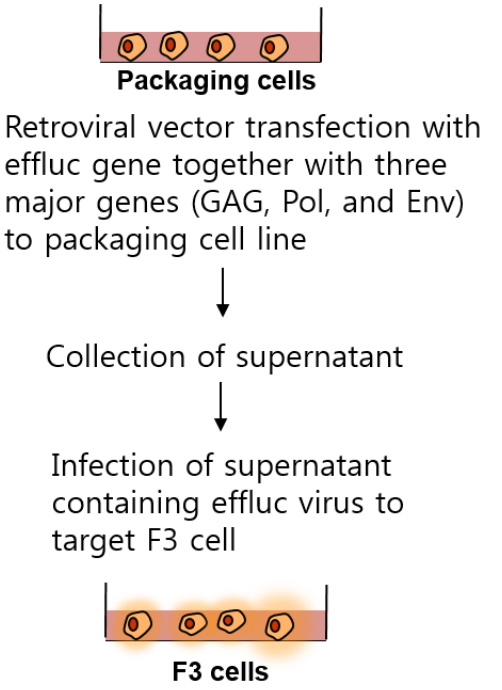

Scanning electron microscopy

The morphology of GO-BC scaffolds was verified using field emission scanning electron microscopy (SEM; JEM-7401F, Joel Ltd, Tokyo, Japan). The sample was rinsed using PBS and dehydrated by soaking at increasing amount of ethanol (30%–100%). Specimens for SEM were covered using gold-palladium alloy onto an aluminum stub after drying in hexamethyldisilazane (HMDS).

Confocal microscopy

2 μg of DiI (Invitrogen) was incubated with 5×10^4 F3-effluc cells to label cells. The cells were centrifuged at 3000 rpm for 5 min. DiI-labeled cells were then seeded on GO-BC scaffold and cultured for 24 h at 37 °C before being fixed using 4% formaldehyde solution (Sigma) while gently shaking for 20 min. After cells were rinsed three times using PBS for 15 min, cells were mounted on cover-slip using mounting solution containing 4′, 6-diamidino-2-phenylindole dihydrochloride (DAPI) (Vector Laboratories, Inc, CA). The fluorescence images were acquired using confocal laser scanning microscopy (Carl Zeiss LSM 510). Blue light (exi. 370 nm/emi. 460 nm) filter was used for DAPI and DiI dye excitation and emission spectra were used in 553 nm and 570 nm, respectively.

Calcium imaging

F3 cells were cultured in 96-well plates with BC or GO-BC for 4 d. On day 4, 1 mM AM ester solution was prepared using DMSO (dimethylsulfoxide). Cells were washed three times with 10 mM HEPES buffer containing 0.5% BSA (bovine serum albumin). 100 μM of the ester solution diluted with HEPES buffer was added to the cells and incubated at 37 °C for 30 min. During the incubation period the plate was protected from light. The cells were then washed three times with 10 mM HEPES buffer containing 0.5% BSA. Fluorescence images were obtained using a fluorescence confocal microscope.

Establishment of corticectomy rat model and implantation of GO-BC/F3-effluc complex

Adult male Sprague-Dawley (SD) weighing 200 g-250 g (7 week old rat) were purchased from OrientBio (Sungnam, Korea). The rats were anesthetized using zoletil 50 (15 mg kg^{-1}, i.p.) mixed with Rompun (10 mg kg^{-1}, i.p.) and were placed in a stereotactic frame to accurately point out the surgical coordinates. After making incisions at the midline scalp and periosteum, the skull was stereotactically removed with an electronic hand drill at the following coordinates: (a) 4 mm rostral/1 mm lateral, (b) 2 mm caudal/1 mm lateral, and (c) 4 mm rostral/6 mm lateral. After removing the tripodal skull, the exposed dura mater and motor cortices were carefully resected with surgical blades, and biopolar electrode was used for hemostasis. Finally, the cavity was filled with absorbable hemostatic gelatin sponge (Ethicon, Somerville, NJ, USA). The incised skin was sutured after complete hemostasis. All animal experiments were approved by Seoul National University Hospital Institutional Animal Care and Use Committee (IACUC NO. 13-2013-001-8). For scaffold/cell implantation, sterile BC or GO-BC scaffolds on ethanol were washed extensively with PBS for the complete removal of ethanol. To incorporate the cell/scaffold complex, 5×10^5 F3-effluc cells were harvested using trypsin, and resuspended in PBS. Then, 10 μl of resuspended F3-effluc cells were seeded into the GO-BC scaffold. Two hours after incubating the F3-effluc/scaffold complex, this complex was implanted into the cavity of the corticectomized rat brain ($n = 4$).

Limb placement behavior test in corticectomized rats

Two types of proprioceptive-response-related behavior tests were conducted to evaluate the corticectomy rat model: the whisker tactile and forelimb tests. Behavioral tests were carried out on the experimental table in a semi-dark, silent room to minimize stimulation or excitation of animals. After complete relaxation, the forelimb test was performed by gently pulling down the forelimb of corticectomized rats to examine the degree of forelimb retraction. The test scores were calculated as follows: 0

for normal retraction and 1–3 for abnormal retraction according to the amount and strength. The whisker tactile test evaluates the level of sensory perception of whisker stimulation. The animal was brought to the table edge, which allows the animal to reach the edge with its fore paw. The rat was scored on whether or not it could reach out its legs to the table when its whiskers were stimulated. Each animal was tested three times, and the scores were calculated as follows: 0 for normal reaching, and 1–3 for abnormal reaching according to the amount of stretching.

In vitro luciferase assay and *in vivo* bioluminescence imaging

For *in vitro* luciferase assay, 5×10^4 F3-effLuc cells were seeded onto GO-BC or BC, and incubated until 0, 1, 2, 4, 8 d before lysed using lysis buffer. The luciferase assay kit (Applied Biosystems, Carlsbad, CA, USA) was used for luciferase-substrate reaction, and luciferase intensity was measured using a Glomax (Promega, Madison, WI, USA). *In vivo* bioluminescence imaging of each group ($n = 4$) followed 0, 1, 2, 4, 8, and 12 d after transplantation. To acquire bioluminescence images, the rats were sedated with 2% isoflurane in 100% O_2 inhaled through a nose cone. D-Luciferin (Caliper Life Sciences, Hopkinton, MA, USA) was diluted to 30 mg ml^{-1} in normal saline and 0.6 mg of D-Luciferin was directly administrated inside the sutured scalp. To suppress the innate immune response against the human F3-effLuc cells, cyclosporine A (5 mg kg^{-1}) was intraperitoneally administered every day after transplantation. *In vivo* bioluminescence imaging system (IVIS-100, Xenogen) equipped with a CCD camera was used for imaging. Images were acquired by integrating light for 30 s while aquired data were quantified and analyzed by LivingImage.

Acquisition of PAI

For *in vivo* PAI of GO-BC/cell complex-implanted mouse, seven-week-old adult male BALB/c-nu mouse weighing 30–40 g were purchased from OrientBio (Sungnam, Kyungki, Korea). After 1.5–2 cm skin incision, GO-BC/cell complex was inserted subcutaneously on the hind thigh before the incised skin was sutured. The BC/cell complex and F3-effLuc cell without scaffold were also implanted as controls. PAI was performed with Vevo LAZR System (VisualSonics Inc., Toronto, Canada) with a laser at the excitation wavelength of 700 nm and photoacoustic gain of 40 db. The PAI region was slathered with ultrasound gel, Aquasonic (Parker, NJ, USA) and photoacoustic/ultrasound probe was contacted for visualization of tomographic image.

Brain sectioning and histological analysis

The anesthetized rats were transcardially perfused using normal saline containing 4% paraformaldehyde (PFA, Sigma-Aldrich). The brains were removed and post-fixed using 4% paraformaldehyde coronally cryosectioned at 14 μm-thickness after dehydration in 10%, 20%, and 30% sucrose at 4 °C. Sections were permeabilized on the glass slides in 0.5% Triton-containing PBS for 5 min, washed using PBS for 5 min. They were then blocked by incubation with 1% normal horse serum for 1 h at room temperature. The slides were incubated overnight in antibody against MAP2 (1:100-dilution, Sigma), or Synaptophysin (1:100-dilution, Abcam). The secondary antibody labeled with alex Fluor 488/555 for MAP2 and synaptophysin was used (purchased from Thermo Fisher Scientific, U.S.) and incubated with tissue sample for 2 h at room temperature. An immunohistochemistry assay was conducted using confocal laser microscopy (LSM 510; Carl Zeiss, Jena, German).

Statistical analysis

The data were obtained from 4 biological replicates and were calculated using the Student's t-test. Statistical significance was accepted at P value of <0.05.

Acknowledgments

F3 human neural stem cell line was kindly provided by Seung U Kim, Chung-Ang University College of Medicine. This research was supported by a grant of the Korea Health Technology R&D Project through the Korea Health Industry Development Institute (KHIDI), funded by the Ministry of Health & Welfare, Republic of Korea (HI14C1277), and National Research Foundation of Korea grant funded by the Korea government (MSIP) (2015M3C7A1028926 and 2017M3C7A1048079), and by Basic Science Research Program through the National Research Foundation of Korea (NRF) funded by the Ministry of Education (2016R1D1A1A02937217) and Priority Research Center Program (2010-0020207) through NRF funded by the Ministry of Education (MOE) and Global Research and Development Center Program (2018K1A4A3A01064272) and Basic Science Research Program (2017R1A2B2010123) through NRF funded by the Ministry of Science and ICT (MSIT).

Conflicts of interest

The authors declare no competing financial interest.

ORCID iDs

Jinho Hyun https://orcid.org/0000-0002-9992-5681
Suklyun Hong https://orcid.org/0000-0001-6504-9209
Byung Hee Hong https://orcid.org/0000-0001-8355-8875

References

[1] Lindvall O, Kokaia Z and Martinez-Serrano A 2014 *Nat. Med.* **10** S42–50

[2] Martino G and Pluchino S 2006 *Nat. Rev. Neurosci.* **7** 395–406
[3] Dimmeler S, Ding S, Rando T A and Trounson A 2014 *Nat. Med.* **20** 814–21
[4] Ziv K and Gambhir S S 2013 *Nat. Mater.* **12** 180–1
[5] Hwang D W *et al* 2014 *PLoS One* **9** e105129
[6] Novoselov K S, Fal'ko V I, Colombo L, Gellert P R, Schwab M G and Kim K A 2012 *Roadmap Graphene Nat.* **490** 192–200
[7] Bae S *et al* 2010 *Nat. Nanotechnol.* **5** 574–8
[8] Li N, Oida S, Tulevski G S, Han S J, Hannon J B, Sadana D K and Chen T C 2013 *Nat. Commun.* **4** 2294
[9] Zhang Y, Nayak T R, Hong H and Cai W 2012 *Nanoscale* **4** 3833–42
[10] Chung C, Kim Y K, Shin D, Ryoo S R, Hong B H and Min D H 2013 *Acc. Chem. Res.* **46** 2211–24
[11] Lu C H, Yang H H, Zhu C L, Chen X and Chen G N 2009 *Angew. Chem., Int. Ed. Engl.* **48** 4785–7
[12] Hong H *et al* 2012 *ACS Nano* **6** 2361–70
[13] Park S Y, Park J, Sim S H, Sung M G, Kim K S, Hong B H and Hong S 2011 *Adv. Mater.* **23** H263–7
[14] Kim J *et al* 2013 *J. Biomed. Mater. Res.* A **1010** 3520–30
[15] Chen G Y, Pang D W, Hwang S M, Tuan H Y and Hu Y C 2012 *Biomaterials* **33** 418–27
[16] Wang Y, Lee W C, Manga K K, Ang P K, Lu J, Liu Y P, Lim C T and Loh K P 2012 *Adv. Mater.* **24** 4285–90
[17] Nayak T R *et al* 2011 *ACS Nano* **5** 4670–8
[18] Solanki A, Chueng S T, Yin P T, Kappera R, Chhowalla M and Lee K B 2013 *Adv. Mater.* **25** 5477–82
[19] Helenius G, Backdahl H, Bodin A, Nannmark U, Gatenholm P and Risberg B 2006 *J. Biomed. Mater. Res.* A **76** 431–8
[20] Zang S, Zhuo Q, Chang X, Qiu G, Wu Z and Yang G 2014 *Carbohydr. Polym.* **104** 158–65
[21] Svensson A, Nicklasson E, Harrah T, Panilaitis B, Kaplan D L, Brittberg M and Gatenholm P 2005 *Biomaterials* **26** 419–31
[22] Klemm D, Schumann D, Udhardt U and Marsch S 2001 *Prog. Polym. Sci.* **26** 1561–603
[23] Zaminpayma E and Mirabbaszadeh K 2012 *Comput. Mater. Sci.* **58** 7–11
[24] Tu Y *et al* 2013 *Nat. Nanotechnol.* **8** 594–601
[25] Engler A J, Sen S, Sweeney H L and Discher D E 2006 *Cell* **126** 677–89
[26] Kim J, Kim S W, Park S, Lim K T, Seonwoo H, Kim Y, Hong B H, Choung Y H and Chung J H 2013 *Adv. Healthc. Mater.* **2** 1525–31
[27] Feng Y, Zhang X, Shen Y, Yoshino K and Feng W A 2012 *Carbohydr. Polym.* **87** 644–9
[28] Park K I, Teng Y D and Snyder E Y 2002 *Nat. Biotechnol.* **20** 1111–7
[29] Wu C, Li J, Pang P, Liu J, Zhu K, Li D, Cheng D, Chen J, Shuai X and Shan H 2014 *Biomaterials* **35** 8249–60
[30] Yang Z, Wang Y, Li Y, Liu Q, Zeng Q and Xu X 2014 *Biotechnology* **14** 55
[31] Kang W J, Kang H J, Kim H S, Chung J K, Lee M C and Lee D S 2006 *J. Nucl. Med.* **47** 1295–301
[32] Vandeputte C *et al* 2014 *Neurobiol. Dis.* **69** 144–55
[33] Yang K, Zhang S, Zhang G, Sun X, Lee S T and Liu Z 2010 *Nano. Lett.* **10** 3318–23
[34] Orive G, Anitua E, Pedraz J L and Emerich D F 2009 *Nat. Rev. Neurosci.* **10** 682–92
[35] Kresse G and Furthmuller J 1996 *Phys. Rev.* B **54** 11169–86
[36] Kresse G and Furthmüller J 1996 *Comput. Mater. Sci.* **6** 15–50
[37] Perdew J P, Burke K and Ernzerhof M 1996 *Phys. Rev. Lett.* **77** 3865–8
[38] Grimme S 2006 *J. Comput. Chem.* **27** 1787–99
[39] Strachan A, van Duin A C, Chakraborty D, Dasgupta S and Goddard W A 2003 *Phys. Rev. Lett.* **91** 098301
[41] Bramini M, Alberinin G, Colombo E, Chiacchiaretta M, DiFrancesco M, Maya-Vetencourt J F, Maragliano L, Benfenati F and Cesca F 2018 *Frontiers Syst. Neurosci.* **12** 12
[42] Zhang Z, Klausen L H, Chen M and Dong M 2018 *Small* **14** 1801983
[43] Dominguez-Bajo A, Gonzalez-Mayorga A, Guerrero C R, Palomares F J, Garica R, Lopez-Dolado E and Serrano M C 2019 *Biomaterials* **192** 461
[44] Lopez-Dolado E, Gonzalez-Mayorga A, Gutierrez M C and Serrano M C 2016 *Biomaterials* **99** 72
[45] Xiao M, Li X, Song Q, Zhang Q, Lazzarino M, Cheng G, Paolo F, Severino U and Torre V 2018 *Adv. Mater.* **30** 1806132
[46] Ma Q, Yang L, Jiang Z, Song Q, Xiao M, Zhang D, Ma X, Wen T and Cheng G 2016 *ACS Appl. Mater. Interfaces* **8** 34227
[47] Castagnola V, Zhao W, Boselli M, Giudice M C L, Meder F, Polo E, Paton K R, Backes C, Coleman J N and Dawson K A 2018 *Nat. Commun.* **9** 1577
[48] Lee W C, Lim C H, Shi H, Tang L A L, Wang Y, Lim C T and Loh K P 2011 *ACS Nano* **5** 7334